ENGINEER - Vol. LIX, No. 02, pp. [61-74], 2026
© The Institution of Engineers, Sri Lanka
DOI: https://doi.org/10.4038/engineer.v59i2.7756

Numerical Investigation of Local Geometric Imperfections on the Seismic Behaviour of Thin-Walled Steel Hollow Piers

A.G.Y.M. Kumara, N.A.I. Ayodya and J.A.S.C. Jayasinghe

Abstract: Steel hollow box piers are widely utilized in modern infrastructure owing to their high strength-to-mass ratio, torsional rigidity, and superior seismic resistance. However, despite these advantages, thin-walled steel sections are susceptible to local buckling under seismic excitation, resulting in notable reductions in strength and ductility when subjected to lateral cyclic loading. Initial geometric imperfections introduced during fabrication, welding, transportation, or assembly significantly affect this behaviour. This study presents a detailed numerical investigation on the influence of Local Geometric Imperfections on the lateral stability, deformation characteristics, and cyclic load-carrying capacity of steel hollow piers. Finite element analyses were conducted using *ABAQUS*, incorporating an elasto-plastic bilinear stress–strain model with combined hardening. LGI profiles derived from buckling mode shapes through eigen value analysis were introduced into the finite element model, which was subsequently subjected to cyclic lateral loading after the application of an initial axial load (P/P_y). The results reveal that local geometric imperfections have a substantial impact on the seismic performance of steel hollow piers, particularly when located within the lower one-third of the pier height, where local buckling typically initiates. The reductions in maximum strength (H_{max}/H_y) and ductility (δ_{max}/δ_y) intensified with increasing slenderness ratio (λ) and axial load ratio (P/P_y), reaching up to 17% in critical conditions. Moreover, limiting the local imperfection amplitude in the bottom one-third region to about 1% of the pier width was found to maintain strength reduction below 10%, ensuring acceptable seismic performance. These findings emphasize the necessity of explicitly accounting for local geometric imperfections in the seismic design and performance evaluation of steel hollow piers.

Keywords: Cyclic loading, FE modelling, Local geometric imperfection, Seismic response, Steel hollow pier

1. Introduction

Modern bridge systems located in seismic regions demand structural components with high strength, stiffness, and superior energy dissipation to maintain performance and safety during strong ground motions. Despite their efficiency and adaptability, steel hollow box piers, like other thin-walled structures, are inherently sensitive to initial imperfections introduced during fabrication, welding, or assembly. Accurately determining appropriate imperfection shapes and magnitudes for these welded box-sections is critical for stability design [1]. These imperfections can generally be classified into three categories: residual stresses, global geometric imperfections, and local geometric imperfections. While residual stresses and global imperfections affect the overall stability and load-carrying behavior, Local Geometric Imperfections (LGIs) have a more direct influence on localized instability such as local buckling during cyclic lateral loading. These LGIs significantly alter the stress distribution, stiffness degradation, and seismic performance of the pier, making their evaluation crucial for accurate design and enhanced structural resilience.

Initial imperfections in steel piers arise during various stages of fabrication and handling, including welding, transportation, assembly, and installation.

Global deviations like coupled deflection and rotation often arise during these handling stages

Eng. A.G.Y.M. Kumara, AMIE(SL), B.Sc. Eng. (Hons) (Peradeniya), Department of Civil Engineering, Faculty of Engineering, University of Peradeniya.
Email: e18183@eng.pdn.ac.lk
https://orcid.org/0009-0005-0374-7219
Eng. N.A.I. Ayodya, AMIE(SL), B.Sc. Eng. (Hons) (Peradeniya), Department of Civil Engineering, Faculty of Engineering, University of Peradeniya.
Email: e18033@eng.pdn.ac.lk
https://orcid.org/0009-0004-3980-5006
Eng. (Dr.) J.A.S.C. Jayasinghe, AMIE(SL), B.Sc. Eng. (Hons) (Peradeniya), M.Eng. (AIT), PhD. (Tokyo), Senior Lecturer in Department of Civil Engineering, University of Peradeniya, Sri Lanka.
Email: supunj@pdn.ac.lk
https://orcid.org/0000_0003_1054_9358

[2-12]. During welding, high thermal gradients and rapid cooling can induce residual stresses that lead to permanent deformations and distortions in the plate elements [13,14]. Furthermore, mechanical vibrations and handling stresses during transportation, as well as misalignments during field assembly, may introduce geometric deviations that compromise the structural performance of the pier. These can manifest as bow, camber, and twist, departing significantly from the perfect member geometry [15]. These imperfections modify both the geometry and stress distribution, ultimately influencing the pier's ability to withstand seismic forces and resist instability.

Among all imperfection types, local geometric imperfections are particularly critical because of their direct influence on the initiation of local buckling in slender plate elements. While idealized specimens are often modeled with perfectly flat and straight plates, real-world fabrication introduces measurable deviations from planarity. Additionally, manufacturing-induced thickness variations can further influence load-carrying capacity [16]. The local buckling shape typically manifests as a half-wave pattern along the height and width of the plate, which is considered the most detrimental to strength and post-buckling performance. However, traditional buckling mode-affine models may not represent the most unfavorable geometric imperfections, which are often load-dependent [17-18]. To quantify these imperfections, measurements can be obtained using a feeler gauge at critical sections such as the top, mid-height, and bottom regions of the pier, as illustrated in Figure 1.

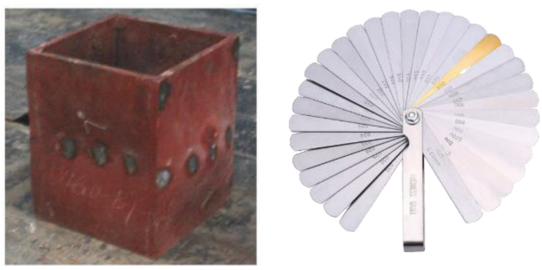

(a) (b)

Figure 1 - Measuring imperfections: (a) Box specimen and (b) feeler gauge [13]

As shown in Figure 2, the overall imperfection profiles are typically represented using trigonometric functions to approximate the measured deformation shapes.

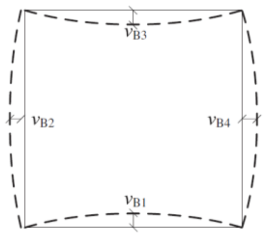

Figure 2 - Measured points of initial geometric imperfections (v_{Bi} is the maximum lateral deformation) [17]

In most cases, the maximum lateral deviation occurs around the mid-height of the plate, closely resembling the expected buckling deformation pattern observed in experimental investigations.

A similar local initial imperfection shape was introduced in the study by Sato *et al., (2014)* [19], where the plate element's initial deflection was defined at five distinct amplitude levels based on fabrication tolerance limits. These deflection profiles were modeled to replicate the locally buckled shapes observed in previous experiments using trigonometric expressions that maintain right-angled intersections at the plate corners. The parameters adopted for the numerical analysis are summarized in Table 1, while the imperfection function introduced into the Finite Element model is illustrated in Figure 3, formulated using Equations (1) and (2) [19].

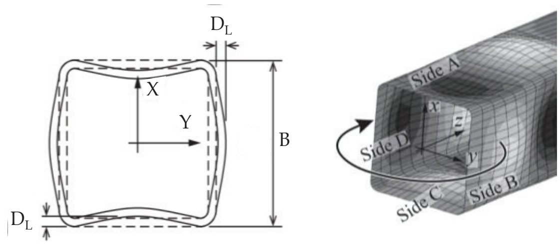

(a) (b)

Figure 3 - Deflection of initial local imperfection: (a) sectional view and (b) 3D view [19]

Table 1 - List of analysis parameters [19]

Item	Parameter
Initial local imperfection D_L	$\frac{1}{10000}, \frac{10}{10000}, \frac{50}{10000}, \frac{100}{10000}, \frac{300}{10000}$

$$u_{x,L} = \mp \frac{D_L . B}{2} . (\cos\frac{2\pi y}{B} + 1) . \sin\frac{\pi z}{B} \qquad ...(1)$$

$$u_{y,L} = \pm \frac{D_L . B}{2} . (\cos\frac{2\pi x}{B} + 1) . \sin\frac{\pi z}{B} \qquad ...(2)$$

$u_{x,L}$ and $u_{y,L}$ denote the initial local deflections in the x- and y-directions of the plate elements, respectively [19]. The British Standards Institution (BSI), through Eurocode 3 [20], places considerable emphasis on the accurate representation of initial imperfections in the structural design and numerical analysis of slender steel members. Among these, Local Geometric Imperfections are particularly significant, as they have a direct influence on the onset of local buckling, post-buckling strength, and energy dissipation capacity of thin-walled steel structures. In practice, these imperfections are inevitable consequences of fabrication, welding, and handling processes, and even minor geometric deviations can lead to substantial variations in the stress field and deformation characteristics. As a result, an appropriate representation of imperfections in analytical or numerical models is crucial to capture the true nonlinear response of the structure under service, ultimate, and seismic loading conditions.

Annex C of Eurocode 3 [20] provides detailed guidelines for the use of the Finite Element Method (FEM) in structural design, with Clause C.2 "Use" highlighting the critical parameters that govern model reliability. It specifies that the accuracy of FEM-based structural analyses depends heavily on the realistic representation of geometry, boundary conditions, material behaviour, loading sequences, and particularly, the inclusion of imperfections. The clause underscores that simplifications or omissions in modelling imperfections may result in non-conservative predictions of load-carrying capacity and stability performance. Therefore, engineers are advised to adopt modelling practices that accurately reproduce the physical characteristics and tolerances of the fabricated structure. Furthermore, the standard allows each National Annex to define specific provisions and permissible limits for imperfections to ensure that regional fabrication practices and construction tolerances are appropriately reflected in numerical simulations.

Clause C.5 "Use of imperfections" provides explicit recommendations for incorporating local geometric imperfections into finite element models. It advocates the introduction of equivalent geometric imperfections that resemble the critical buckling mode shapes or the characteristic local deformation profiles of plate elements. To maintain consistency with practical fabrication tolerances, Eurocode 3 [20] recommends using an imperfection amplitude of approximately 80% of the geometric tolerance specified for the component. This approach achieves a balance between conservatism and realism, allowing the model to reflect potential weaknesses without overestimating the severity of imperfections. The orientation and direction of the imperfections should also be selected to generate the most unfavourable structural response, particularly in regions subjected to high compressive stresses, such as the base of steel hollow piers under lateral cyclic or seismic loading [20].

Table 2 and Figure 4 provide reference data and illustrative guidance for defining imperfection amplitudes, orientations, and spatial distributions. These standardized references contribute to a consistent modelling framework across studies and design applications, facilitating accurate simulation of buckling initiation, strength degradation, and post-buckling stiffness reduction. Ultimately, adherence to these provisions ensures that finite element analyses can yield reliable and physically representative predictions of the seismic and stability performance of thin-walled steel structures.

Table 2 - Equivalent geometric imperfections [20]

Type of imperfection	Component	Shape	Magnitude
Local	Panel or subpanel with short span *a* or *b*	Buckling shape	Min (a/200, b/200)
Local	Stiffener or flange subject to twist	Bow twist	1/50

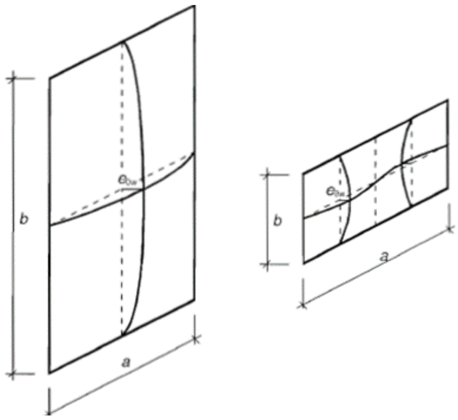

Figure 4 - Modelling of equivalent geometric imperfections: Local panel or subpanel [20]

Although many studies have addressed the effects of imperfections in steel structures, the influence of local geometric imperfections on the seismic performance of thin-walled steel hollow piers has not yet been thoroughly investigated. Therefore, the present study aims to provide a comprehensive numerical evaluation of this effect. A detailed FE model was developed using *ABAQUS* software and validated against the experimental results reported by Susantha *et al., (2007)* [21]. Subsequent parametric analyses were performed to examine the sensitivity of seismic performance to variations in local imperfection amplitude.

A series of local imperfection profiles, with progressively increasing deflection amplitudes derived from Sato *et al., (2014)* [19], were applied to the FE model to simulate realistic fabrication deviations. These profiles were analyzed both within and beyond the permissible tolerance limits to investigate their influence on the global and local response of the structure. The primary objective was to understand how the magnitude of these imperfections influences the strength and ductility of the pier, while also providing quantitative insights to support improved seismic design guidelines and assessment procedures.

To achieve this, the study evaluated key performance indicators such as normalized ductility (δ_{max}/δ_y) and normalized maximum strength capacity (H_{max}/H_y), where δ_y and H_y represent the yield displacement and yield load, respectively, as determined using Equations (3) and (4). By comparing these parameters under various imperfection scenarios, the relationship between imperfection severity and seismic performance was systematically analyzed. In addition, the influence of design parameters such as the axial load ratio (P/P_y), width-to-thickness ratio (R_f), and slenderness ratio (λ) was also examined to understand their combined effects with local imperfections. This research provides valuable insight into how local geometric imperfections influence the seismic behavior of thin-walled steel hollow piers, supporting performance-based seismic design and structural optimization.

2. Methodology

A systematic research methodology was formulated to address the identified gaps and support a detailed parametric investigation. The study began with an extensive review of existing literature on initial imperfections in steel structures, which provided the foundation for developing a reliable FE model. The FE model was then validated to ensure its accuracy in representing the structural behaviour of thin-walled steel hollow piers under cyclic loading conditions.

After validation, a comprehensive numerical parametric study was conducted to investigate the influence of Local Geometric Imperfections on the seismic performance of steel hollow piers. The methodology followed a step-by-step approach from defining model parameters and boundary conditions to analysing the response of imperfect models under cyclic loading. This structured approach ensured consistency between model development, analysis, and the study's primary objective of understanding the impact of Local Geometric Imperfections on structural performance and improving predictive confidence in seismic response evaluation.

2.1 Numerical Modelling

The numerical modelling phase aimed to simulate the seismic behaviour of thin-walled steel hollow piers through advanced finite element analysis in *ABAQUS*. Material properties, yielding criteria, and hardening models were defined using validated experimental data and previous studies. The pier geometry, including overall dimensions, diaphragm configurations, and boundary conditions, reflected realistic bridge conditions under seismic loading. A perfect model without imperfections served as the reference, while subsequent models incorporated local geometric imperfections derived from eigenvalue buckling analysis to replicate realistic deformation patterns. Different imperfection amplitudes were applied to examine their effects on local buckling, stiffness degradation, strength reduction, and ductility. This modelling approach provided a comprehensive understanding of how imperfection magnitude and location govern the seismic performance of steel piers, supporting reliable interpretation of numerical results and improving confidence in seismic design assessments.

2.1.1 Material properties

In this study, material properties of steel, including yield stress, ultimate stress, Young's modulus, and Poisson's ratio, were defined to accurately represent its elastic and plastic behavior. A combined hardening model was adopted, which incorporates the von Mises yield criterion together with an associated plastic flow rule to capture the inelastic response of steel under cyclic loading conditions [22]. The type of steel used in this investigation is SM490, classified under the Japanese Industrial Standards (JIS), as reported by Susantha *et al., (2005)* [3]. The detailed material properties consistent with that study are summarized in Table 3.

To maintain computational efficiency while ensuring reliable accuracy, a simplified bilinear stress–strain relationship, illustrated in Figure 5, was used in the analysis. This model captures the essential characteristics of steel behavior under cyclic loading without adding unnecessary computational complexity and has been widely adopted in similar numerical investigations.

Table 3 - Material properties [3]

Parameters	Values
Yield stress (σ_y)	412 MPa
Young's modulus (E_s)	206000 MPa
Ultimate stress (σ_u)	650 MPa
Poisson's ratio (v)	0.276

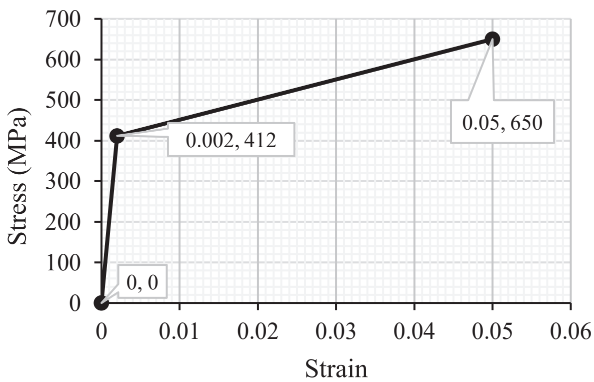

Figure 5 - Bilinear stress-strain steel model

2.1.2 Geometric details of columns

Figure 6 shows the longitudinal dimensions of the modelled pier in a 3D view, illustrating the cross-sectional and diaphragm details. The same cross-sectional properties were used for model validation and the study on local geometric imperfections, while the parametric analysis included variations in cross-sectional dimensions and pier heights.

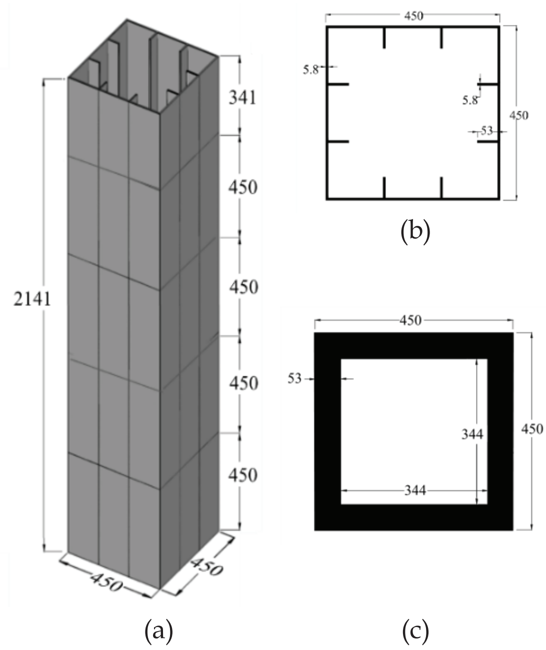

Figure 6 - Dimensions of modelled pier: (a) longitudinal, (b) cross-section and (c) intermediate diaphragms (all dimensions are in millimetres) [21]

2.1.3 Loading procedure

The loading configuration employed in this study initiates with the application of an axial force (P) to simulate the load transmitted from the superstructure. Subsequently, unidirectional cyclic lateral loads are applied. The axial force (P) is expressed as a ratio (P/P_y), where P_y denotes the axial load corresponding to the yield stress of steel for the considered cross-section. In this analysis, the ratio was maintained at 0.2. A unidirectional cyclic load, applied as displacement and varying according to the pattern illustrated in Figure 7, was imposed at the top of the model to represent a simplified seismic loading condition, while the axial load was kept constant throughout the process, as shown in Figure 8.

![]
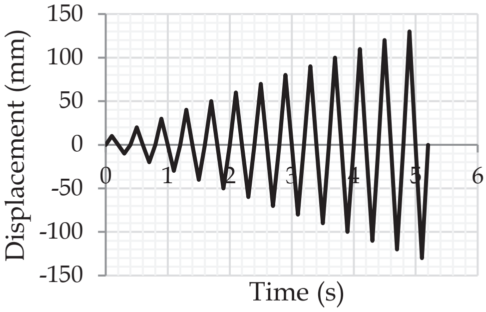

Figure 7 - Displacement history of Uni-directional Cyclic loading

A "perfect model," excluding any initial imperfections, was developed to serve as a reference for comparison with the models incorporating initial imperfections. In this model, the box pier, longitudinal stiffeners, and diaphragms were modelled using four-node shell elements with reduced integration (S4R) and five integration points through the thickness. A fixed boundary condition was assigned at the base, while axial and lateral cyclic loads were applied through a reference point connected rigidly to the top of the column. Previous studies have shown that for square box columns composed of thin-walled steel, local buckling commonly occurs between the base and the bottom diaphragm near the column base [23-26]. The entire pier was meshed using S4R elements with a 25 mm element size, as illustrated in Figure 9. Mesh convergence analysis confirmed that this mesh density achieved sufficient accuracy while maintaining computational efficiency.

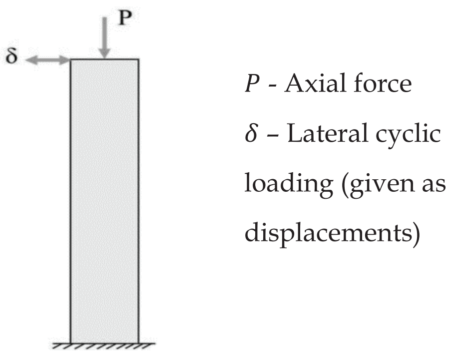

Figure 8 - Loading arrangement

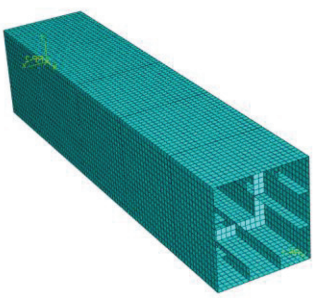

Figure 9 - Numerical model of the steel pier

2.2 Numerical Model with Local Geometric Imperfections

To evaluate the influence of local initial geometric imperfections, the eigenvalue frequency analysis method, as described in Section 2.1, was employed to generate local imperfection profiles. For the parametric study, the most realistic and commonly observed local geometric imperfection shapes, as reported by Sato *et al., (2014)* [19], were incorporated. The local imperfection profiles derived for the test pier in this study, based on the eigenvalue frequency analysis, are illustrated in Figure 10. The primary objective of this parametric investigation is to examine the impact of these local geometric imperfections on the seismic performance of steel piers.

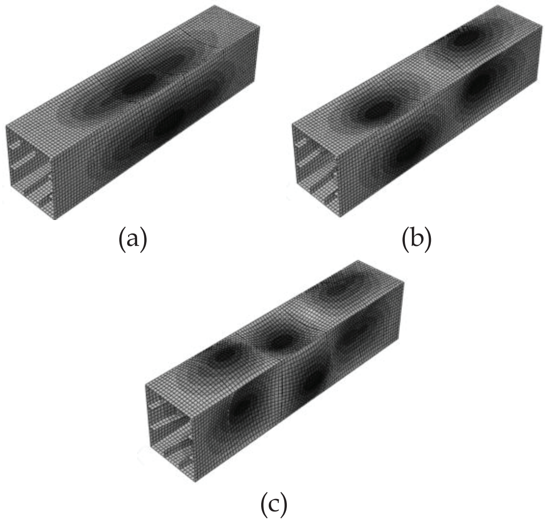

Figure 10 - Local imperfection profiles (a) profile 1, (b) profile 2 and (c) profile 3

For the case of local geometric imperfections, the parametric study investigates the magnitude of imperfections that significantly influence the seismic performance, as summarized in Table 4. The initial imperfection shapes obtained from the eigenvalue analysis are amplified by specific percentage factors to introduce a realistic level of local deformation in each plate. This is illustrated in Figure 11. By amplifying the eigenvalue-derived imperfection modes, the study aims to replicate practical local imperfections that may arise during fabrication or service. This approach ensures that the numerical models realistically capture the potential influence of such imperfections on the seismic response of the piers.

According to Sato *et al., (2014)* [19], the maximum allowable flatness deviation for each flat plate is within ±1.0% or ±3.0 mm. In this analysis, a flatness deviation of 3 mm was selected within this permissible range. To achieve this level of flatness, the initial deflections obtained from the eigenvalue analysis (as listed in the second column of Table 4) were amplified by factors of 19.2, 19.5 and 19.0 for each respective profile. Subsequently, the flatness was increased by 1%, 2%, 3%, 4%, and 5%, corresponding to maximum deflections of 4.5 mm, 9.0 mm, 13.5 mm, 18.0 mm, and 22.5 mm, respectively. These variations were introduced to examine the influence of local geometric imperfections on key design parameters, namely the axial load ratio (P/P_y), width-to-thickness ratio (R_f), and slenderness ratio (λ).

Table 4 - Parametric study for deflection of the plate

LGI Profiles	Maximum DL before amplifying (mm)	Amplifying Factor					
		3 mm	1% (4.5 mm)	2% (9.0 mm)	3% (13.5 mm)	4% (18.0 mm)	5% (22.5 mm)
1	0.1565	19.2	28.8	57.5	86.3	115	143.8
2	0.154	19.5	29.2	58.4	87.7	116.9	146.1
3	0.1577	19	28.5	57.1	85.6	114.1	142.7

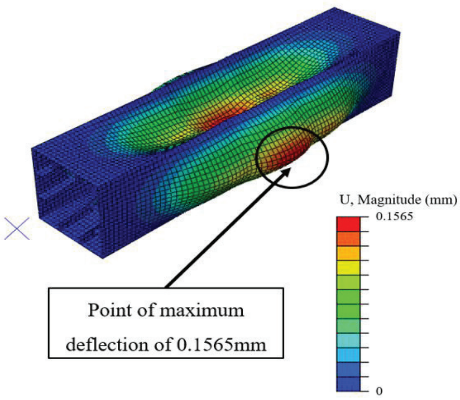

Figure 11 - Selection of maximum deflection of the plate (Exaggerated view)

Table 5 presents the details of the parametric study conducted to investigate the influence of local geometric imperfections on the key design parameters discussed previously. By varying the magnitude of imperfections, as summarized in Table 4, corresponding changes were observed in these design parameters. The numerical models developed based on the different design parameter combinations are summarized in Tables 6 and 7.

Table 5 - The selected values for the parametric study for design parameters

Width to thickness ratio - R_f	Slenderness ratio - λ	Applied axial load to yield load ratio - P/P_y
0.5	0.3	0.15
0.6	0.4	
0.7	0.5	0.20
0.8	0.6	

Tables 6 and 7 present the values corresponding to different design conditions. For these 32 models, the selected imperfection profiles were generated and analysed to evaluate their effects using the developed methodology. To determine the design values required for modelling, Equations (3) and (4) from Susantha *et al., (2007)* [21] were applied.

$$\delta_y = \frac{H_y\, h^3}{3EI} \qquad ...(3)$$

$$H_y = \frac{M_y}{h}\,(1 - \frac{P}{P_y}) \qquad ...(4)$$

where,

δ_y: Yield displacement
M_y: Yield moment of the section
h: Column height
E: Young's modulus
I: Moment of inertia
P: Axial load
P_y: Axial yield load of the section
H_y: Yield Load

Table 6 - Essential values for modelling (P/P_y=0.15)

No	P/P_y	R_f	λ	P(kN)	δ_y	H_y/(kN)
1	0.15	0.50	0.30	905.51	10.75	469.06
2	0.15	0.50	0.40	905.51	18.70	343.61
3	0.15	0.50	0.50	905.51	28.38	266.70
4	0.15	0.50	0.60	905.51	39.30	214.46
5	0.15	0.60	0.30	795.49	10.82	409.93
6	0.15	0.60	0.40	795.49	18.85	300.08
7	0.15	0.60	0.50	795.49	28.55	233.24
8	0.15	0.60	0.60	795.49	39.68	187.13
9	0.15	0.70	0.30	691.05	10.70	353.03
10	0.15	0.70	0.40	691.05	18.50	259.54
11	0.15	0.70	0.50	691.05	28.14	201.18
12	0.15	0.70	0.60	691.05	39.03	161.61
13	0.15	0.80	0.30	606.96	10.42	308.77

14	0.15	0.80	0.40	606.96	18.11	226.35
15	0.15	0.80	0.50	606.96	27.47	175.77
16	0.15	0.80	0.60	606.96	38.12	141.16

Table 7 - Essential values for modelling (P/P_y=0.20)

No	P/P_y	R_f	λ	$P(kN)$	δ_y	$H_y/(kN)$
17	0.20	0.50	0.30	1207.34	10.17	443.78
18	0.20	0.50	0.40	1207.34	17.54	322.30
19	0.20	0.50	0.50	1207.34	26.32	247.32
20	0.20	0.50	0.60	1207.34	35.93	196.03
21	0.20	0.60	0.30	1060.65	10.24	387.84
22	0.20	0.60	0.40	1060.65	17.69	281.48
23	0.20	0.60	0.50	1060.65	26.48	216.31
24	0.20	0.60	0.60	1060.65	36.27	171.04
25	0.20	0.70	0.30	921.40	10.12	333.99
26	0.20	0.70	0.40	921.40	17.35	243.46
27	0.20	0.70	0.50	921.40	26.09	186.56
28	0.20	0.70	0.60	921.40	35.67	147.71
29	0.20	0.80	0.30	809.29	9.86	292.13
30	0.20	0.80	0.40	809.29	16.99	212.32
31	0.20	0.80	0.50	809.29	25.47	163.01
32	0.20	0.80	0.60	809.29	34.84	129.02

3. Results

3.1 Validation of the FEM Model

The influence of mesh density on result accuracy was evaluated through a mesh sensitivity analysis. Figure 12 illustrates the variation in stress at a selected point at the base of the pier for mesh sizes ranging from 50 mm to 10 mm, demonstrating that finer meshes produce more stable and reliable results. Based on this assessment, a 25 mm mesh size was selected as the optimal configuration for this study, ensuring a balance between computational efficiency and accuracy.

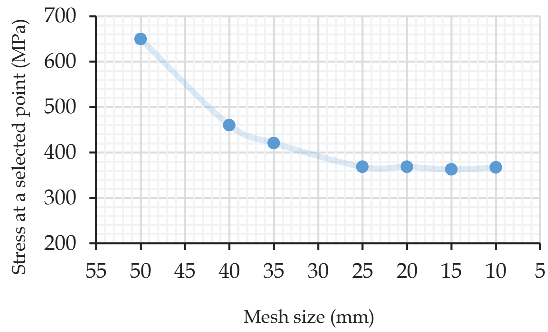

Figure 12 - Variation of base stress with size of the mesh

The loading pattern illustrated in Figure 7 was applied to the steel hollow column for model validation, using the experimental data reported by Susantha *et al., (2007)* [21] as a reference. The envelope curve of the FEM numerical model, presented in Figure 13, shows good agreement with the corresponding experimental results, confirming the accuracy and reliability of the developed model.

Furthermore, the deformation patterns obtained from the numerical analysis closely matched those observed in the experimental study. Figure 14 presents a comparison between the buckling shape at the fixed base reported by Susantha *et al., (2007)* [21] and that of the perfect numerical model, demonstrating a high level of consistency between the two results.

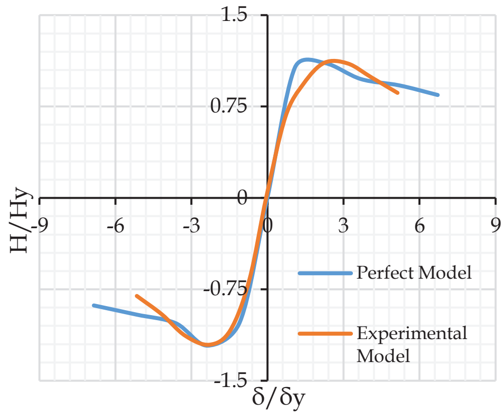

Figure 13 - Comparison of Numerical Model and Experimental model

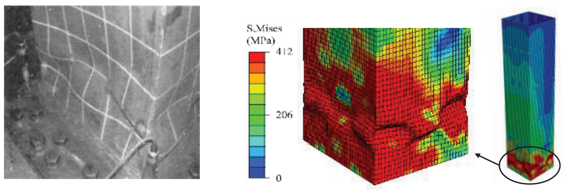

(a) (b)

Figure 14 - Buckling behavior: (a) experimental model and (b) numerical mode [21]

3.2 Results of Local Geometric Imperfections Study

This section presents the outcomes of three parametric studies carried out to investigate the influence of local geometric imperfections on the seismic performance of steel piers. The first study focuses on imperfections within the allowable limits specified by Sato *et al., (2014)* [19], while the second extends beyond this range to represent severe imperfection conditions. The final part of the analysis examines the overall impact of local imperfections on key design parameters and their implications for seismic design practice.

In the first parametric study, the analysis considers imperfections within the permissible range. As outlined in Section 2.2, a maximum local geometric imperfection of 3 mm was adopted based on the recommended upper limit. The results corresponding to this case are illustrated in Figure 15, highlighting the corresponding changes in strength, stiffness degradation, and hysteretic response characteristics.

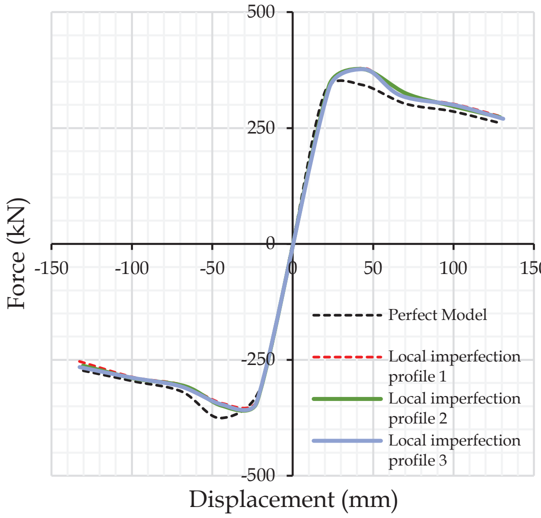

Figure 15 - Comparison of the perfect model performance and local imperfection model performance within the permissible range

As illustrated in Figure 15, within the permissible range, the effect of local geometric imperfections on seismic performance is not visibly significant. Therefore, to identify the threshold at which imperfections begin to have a noticeable impact, it was necessary to extend the analysis beyond the allowable limit (>3 mm). This formed the basis of the second stage of the parametric study.

In this stage, the analysis aimed to determine the magnitude of local imperfections that produce a considerable influence on the seismic behaviour of the structure. According to Table 4, the maximum deflections of the local imperfection profiles were set to 4.5 mm (1%), 9 mm (2%), 13.5 mm (3%), 18 mm (4%), and 22.5 mm (5%). The comparison of the hysteretic curves corresponding to each model is presented in Figures 16 to 18.

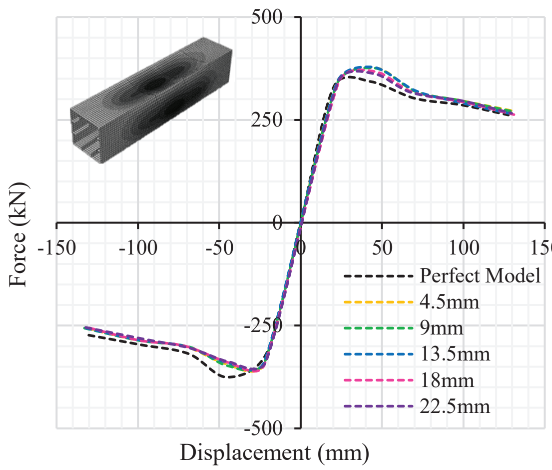

Figure 16 - Comparison of each local imperfection profiles beyond the permissible range, 4.5mm, 9mm, 13.5mm, 18mm and 22.5mm with Perfect model results LI Profile 1

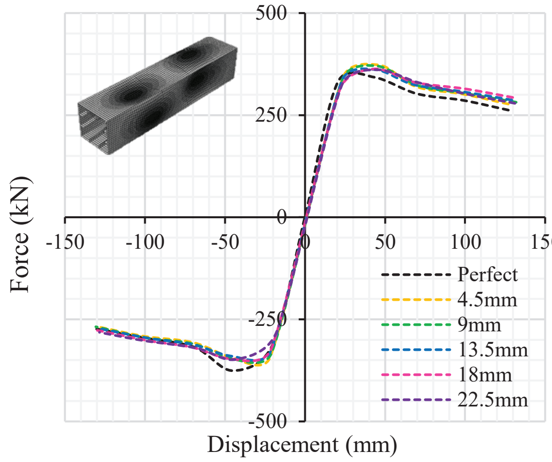

Figure 17 - Comparison of each local imperfection profiles beyond the permissible range, 4.5mm, 9mm, 13.5mm, 18mm and 22.5mm with Perfect model results LI Profile 2

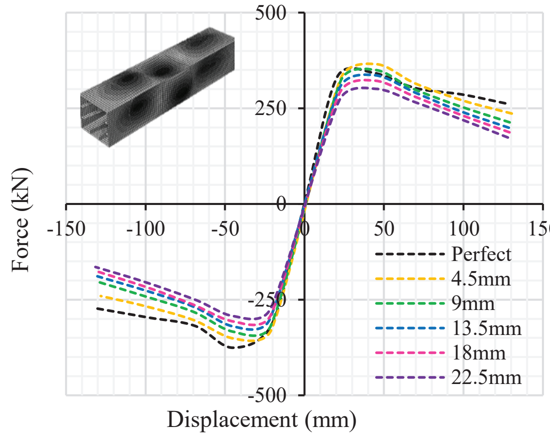

Figure 18 - Comparison of each local imperfection profiles beyond the permissible range, 4.5mm, 9mm, 13.5mm, 18mm and 22.5mm with Perfect model results LI Profile 3

According to the second parametric study shown in Figures 16 to 18, the severity of local geometric imperfections increases when they are concentrated near the bottom region of the pier, where local buckling typically initiates under cyclic loading. Among the tested imperfection amplitudes, 4.5 mm and 9 mm, corresponding to 1% and 2% beyond the permissible flatness limit of ±3 mm, showed a significant influence on seismic performance, particularly for LI Profile 3. These values were therefore identified as critical thresholds and selected for further analysis in the third parametric study.

In the third stage, results were expressed in normalized form, with parameters provided in Tables 6 and 7. Figure 19 shows the variation of δ_{max}/δ_y for P/P_y = 0.15 and 0.20 for LI Profile 3 with a 1% imperfection. No clear trend is observed with λ, while greater variation occurs with increasing P/P_y.

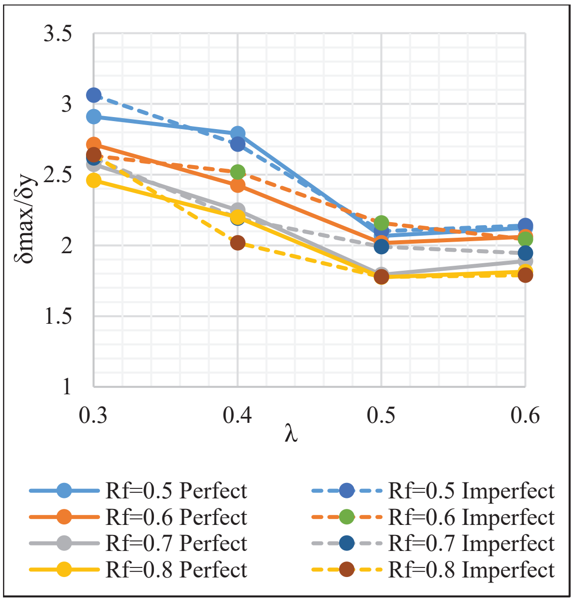

(a)

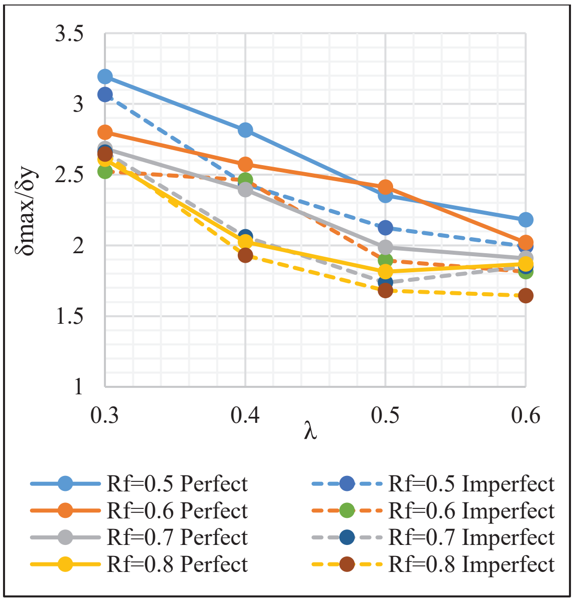

(b)

Figure 19 - δ_{max}/δ_y variation comparison with P/P_y values-LI profile 3 – 1 % imperfection (a) P/P_y=0.15 and (b) P/P_y=0.20

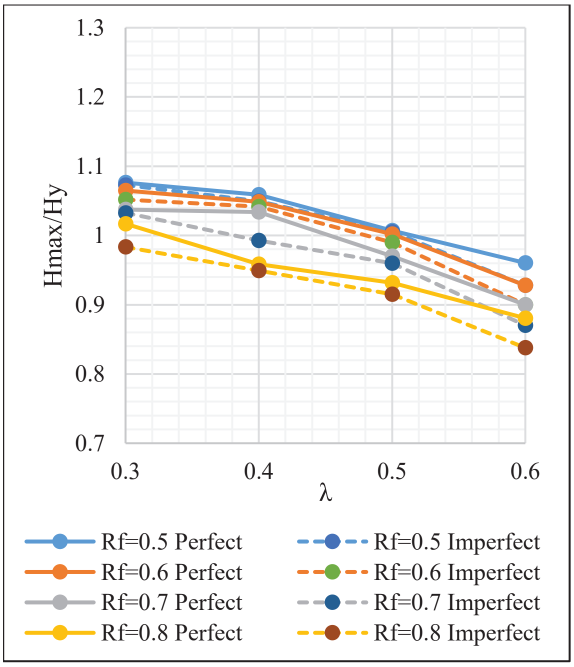

(a)

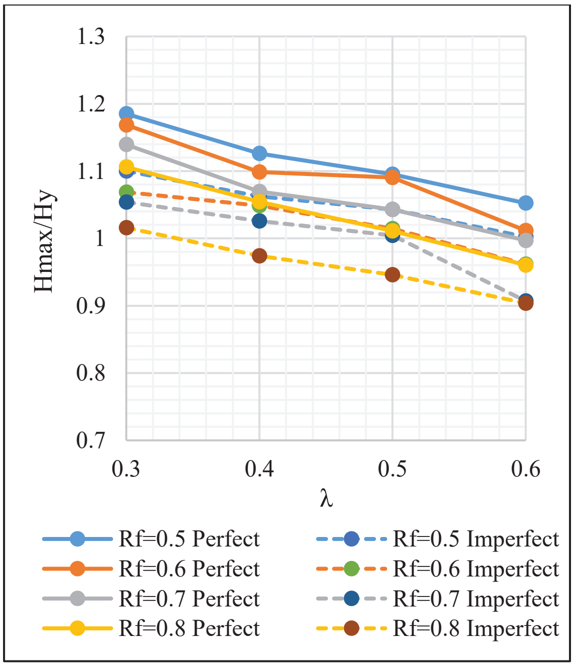

(b)

Figure 20 - H_{max}/H_y variation comparison with P/P_y values-LI profile 3 – 1% imperfection (a) P/P_y=0.15 and (b) P/P_y=0.20

Figure 20 presents the variation of H_{max}/H_y with different λ values for both P/P_y = 0.15 and P/P_y = 0.20 corresponding to LI Profile 3 with a 1% imperfection. The results indicate a reduction in H_{max}/H_y due to the influence of local geometric imperfections, and this reduction becomes more pronounced as the P/P_y ratio increases. Table 8 supports this observation by providing the percentage reduction in H_{max}/H_y values, illustrating the increasing impact of local imperfections with higher P/P_y ratios. For LI Profile 3 with a 2% imperfection, the variation of ductility with different λ values and the comparison between P/P_y = 0.15 and P/P_y = 0.20 are presented in Figure 21. Similar to the 1% imperfection case, no distinct trend in ductility variation is observed, indicating that the influence of λ on ductility remains minimal under this imperfection condition.

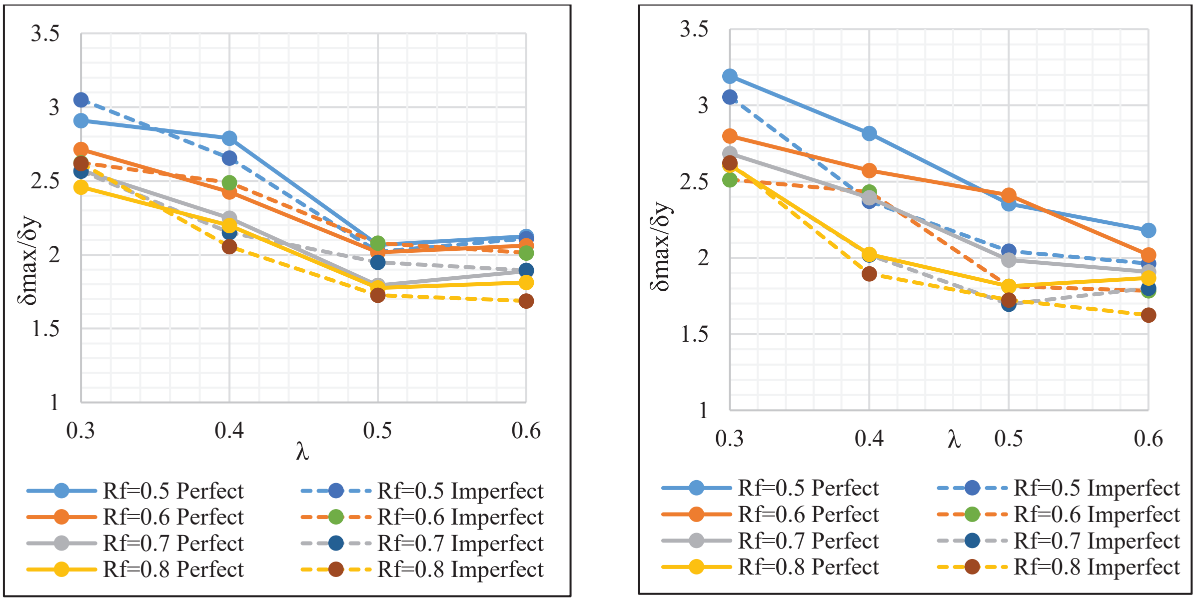

(a) (b)

Figure 21 - $\boldsymbol{\delta_{max}/\delta_y}$ variation comparison with $\boldsymbol{P/P_y}$ values-LI profile 3 – 2% imperfection (a) $\boldsymbol{P/P_y}$=0.15 and (b) $\boldsymbol{P/P_y}$=0.20

Table 8 - Percentage of reduction in $\boldsymbol{H_{max}/H_y}$ for LI profile 3 – 1% imperfection

R_f	λ	P/P_y=0.15			P/P_y=0.20		
		Perfect	Imperfect	% Reduction	Perfect	Imperfect	% Reduction
0.5	0.3	1.08	1.07	**0.33**	1.18	1.10	**7.17**
	0.4	1.06	1.05	**0.85**	1.13	1.06	**5.63**
	0.5	1.01	1.01	**0.18**	1.10	1.04	**4.75**
	0.6	0.96	0.93	**3.38**	1.05	1.00	**4.75**
0.6	0.3	1.06	1.05	**1.23**	1.17	1.07	**8.56**
	0.4	1.05	1.04	**0.66**	1.10	1.05	**4.55**
	0.5	1.00	0.99	**1.19**	1.09	1.01	**6.97**
	0.6	0.93	0.90	**3.00**	1.01	0.96	**4.94**
0.7	0.3	1.04	1.03	**0.45**	1.14	1.05	**7.49**
	0.4	1.03	0.99	**3.99**	1.07	1.03	**4.11**
	0.5	0.97	0.96	**1.03**	1.04	1.00	**3.69**
	0.6	0.90	0.87	**3.33**	1.00	0.91	**9.03**
0.8	0.3	1.02	0.98	**3.30**	1.11	1.02	**8.14**
	0.4	0.96	0.95	**0.97**	1.05	0.97	**7.59**
	0.5	0.93	0.91	**1.80**	1.01	0.95	**6.43**
	0.6	0.88	0.84	**4.87**	0.96	0.90	**5.91**

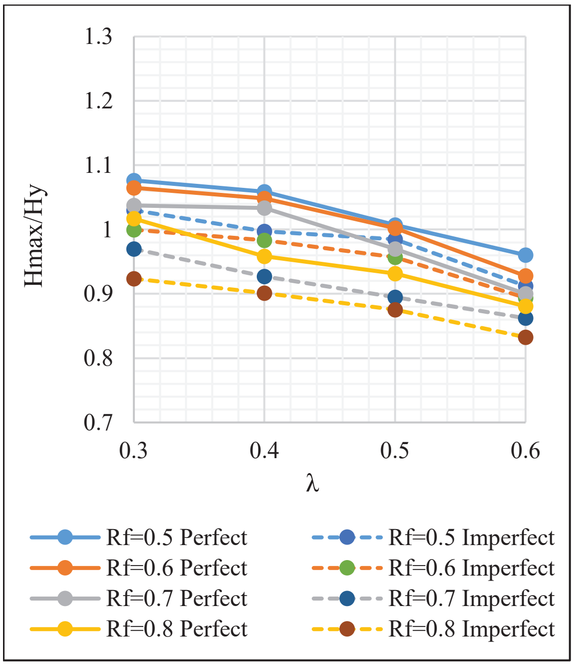

(a)

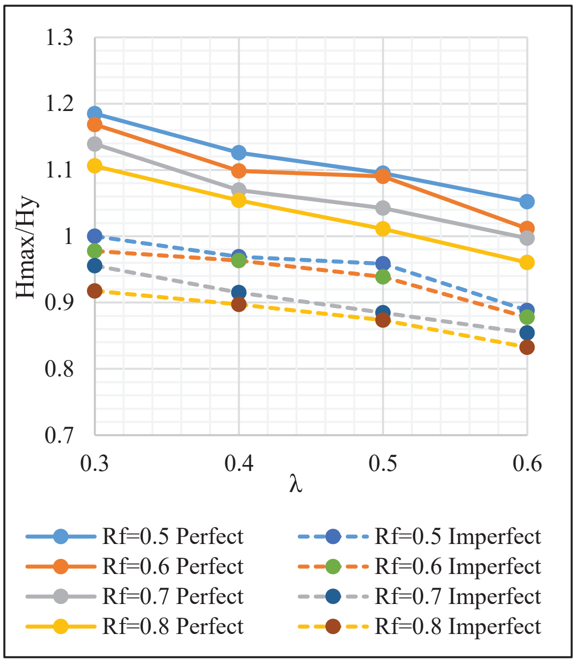

(b)

Figure 22 - H_{max}/H_y variation comparison with P/P_y values–LI profile 3 – 2% imperfection (a) P/P_y=0.15 and (b) P/P_y=0.20

According to Figure 22, the variation of H_{max}/H_y with different λ values, along with the comparison between $P/P_y = 0.15$ and $P/P_y = 0.20$, can be observed. The results indicate that H_{max}/H_y generally decreases as λ increases, and this reduction becomes more significant at higher P/P_y ratios.

Furthermore, the percentage reductions in H_{max}/H_y presented in Table 9 reinforce this finding, confirming the increasing influence of both slenderness and axial load ratio on the reduction of lateral strength.

Table 9 - Percentage of reduction in H_{max}/H_y for LI profile 3 – 2% imperfection

R_f	λ	P/P_y=0.15			P/P_y=0.20		
		Perfect	Imperfect	% reduction	Perfect	Imperfect	% reduction
0.5	0.3	1.08	1.03	**4.30**	1.18	1.00	**15.61**
	0.4	1.06	1.00	**5.79**	1.13	0.97	**13.91**
	0.5	1.01	0.98	**2.23**	1.10	0.96	**12.45**
	0.6	0.96	0.91	**5.01**	1.05	0.89	**15.59**
0.6	0.3	1.06	1.00	**6.12**	1.17	0.98	**16.34**
	0.4	1.05	0.98	**6.22**	1.10	0.96	**12.31**
	0.5	1.00	0.96	**4.51**	1.09	0.94	**13.90**
	0.6	0.93	0.89	**3.67**	1.01	0.88	**13.23**
0.7	0.3	1.04	0.97	**6.52**	1.14	0.96	**16.11**
	0.4	1.03	0.93	**10.30**	1.07	0.92	**14.43**
	0.5	0.97	0.89	**7.76**	1.04	0.88	**15.15**
	0.6	0.90	0.86	**4.20**	1.00	0.85	**14.32**
0.8	0.3	1.02	0.92	**9.18**	1.11	0.92	**17.04**
	0.4	0.96	0.90	**5.94**	1.05	0.90	**14.87**
	0.5	0.93	0.88	**6.05**	1.01	0.87	**13.63**
	0.6	0.88	0.83	**5.46**	0.96	0.83	**13.31**

From Tables 10 and 13, the percentage reductions in H_{max}/H_y for the two levels of local imperfections can be observed. These reductions indicate that increasing R_f and P/P_y values significantly influence the seismic performance of the pier. Among the profiles, LI Profile 3 exhibits the greatest reduction in H_{max}/H_y compared to Profiles 1 and 2. Furthermore, when comparing the 1% and 2% imperfection levels in LI Profile 3, the 2% imperfection results in up to 17% strength reduction under the most critical conditions, whereas the 1% imperfection produces only a 9% reduction. This can be attributed to the fact that Profile 3 induces more severe deformation at the bottom of the pier, which is the most critical region for box piers. Since local buckling typically initiates at the base during lateral cyclic loading, Profile 3 is particularly critical. Therefore, it can be concluded that local imperfections, especially those affecting regions prone to local buckling, have a significant impact on the seismic performance and potential failure of the pier.

4. Conclusions

The following section summarizes the key findings obtained from the analysis of local geometric imperfections and their effects on the seismic performance of steel hollow piers. These conclusions are based on the outcomes of the parametric studies conducted in this research, emphasizing how local imperfection influence the overall seismic response of the piers. The findings also provide a basis for future investigations into the combined and more complex effects of multiple imperfections.

- Local geometric imperfections have the most significant impact on the seismic performance of steel hollow piers when they are located within the lower one-third region of the pier. This finding aligns with the typical failure behavior of steel box sections, where local buckling predominantly initiates near the base under seismic loading.
- The effect of local geometric imperfections becomes more pronounced with increasing slenderness ratio (λ) and axial load ratio (P/P_y), resulting in notable reductions in both strength (up to 17%) and ductility. These parameters therefore play a crucial role in determining the sensitivity of the pier's seismic response.
- For the seismic design of steel hollow piers, the allowable local imperfection in the lower one-third of the pier should be limited to approximately 1% of the pier width. This ensures that the reduction in strength remains below 10%.

Acknowledgement

University Research Grant, URG/2024/14/E of the University of Peradeniya, is highly appreciated.

References

1. Radwan, M. and Kövesdi, B., 2021, December. Local Plate Buckling Type Imperfections for NSS and HSS Welded Box-Section Columns. In *Structures* (Vol. 34, pp. 2628-2643). Elsevier. https://doi.org/10.1016/j.istruc.2021.09.011

2. Kearns, W.H., Weisman, C. and American Welding Society (1976). *Welding handbook*. Miami, Fla.: American Welding Society.

3. Aoki, T. and Susantha, K.A.S. (2005). Seismic Performance of Rectangular-Shaped Steel Piers under Cyclic Loading. *Journal of Structural Engineering*, 131(2), pp.240–249. doi: https://doi.org/10.1061/(asce)0733-9445(2005)131:2(240).

4. Chen, B.-Q. and C. Guedes Soares (2021). Experimental and Numerical Investigation on Welding Simulation of Long Stiffened Steel Plate Specimen. *Marine Structures*, 75, pp.102824–102824. doi: https://doi.org/10.1016/j.marstruc.2020.102824.

5. Chen, S., Xie, X. and Hanqing Zhuge (2019). Hysteretic Model for Steel Piers Considering the Local Buckling of Steel Plates. 183, pp.303–318. doi: https://doi.org/10.1016/j.engstruct.2018.12.101.

6. Dang, J., Yuan, H., Igarashi, A. and Aoki, T. (2017). Multiple-Spring Model for Square-Section Steel Bridge Columns under Bidirectional Seismic Load. *Journal of Structural Engineering*, 143(5), p.04017005. doi: https://doi.org/10.1061/(asce)st.1943-541x.0001735.

7. Haffar, M.Z., Kövesdi, B. and Adany, S. (2021). Buckling of Compressed Plates with Closed-Section Longitudinal Stiffeners: Two New Mathematical Models for Resistance Prediction. *Structures*, 33, pp.3526–3539. doi: https://doi.org/10.1016/j.istruc.2021.06.083.

8. Hassan, M.S., Salawdeh, S. and Goggins, J. (2018). Determination of Geometrical Imperfection Models in Finite Element Analysis of Structural Steel Hollow Sections Under Cyclic Axial

Loading. *Journal of Constructional Steel Research*, 141, pp.189–203. doi: https://doi.org/10.1016/j.jcsr.2017.11.012.

9. Hsu, H. and Juang, J.-L. (2000). Performance of Thin-Walled Box Columns Strengthened with Internal Braces. *Thin-Walled Structures*, 37(3), pp.241–258. doi: https://doi.org/10.1016/s0263-8231(00)00020-3.

10. Jenothan, M., Jayasinghe, J.A.S.C. and Bandara, C.S. (2023). Lateral Behaviour and Performance Evaluation of Steel Piers under Cyclic Lateral Loading. *Journal of Constructional Steel Research*, 201, p.107764. doi: https: //doi.org/10.1016/j.jcsr.2022.107764

11. Lang, Y., Qin, Y., Guo, T., Shu, G., Liu, J., Liu, Z. and Yan, X., 2026. Initial Global Imperfections of L-Shaped Double Steel Plate Composite Walls. *Journal of Constructional Steel Research*, *240*, p.110282. https://doi.org/10.1016/j.jcsr.2026.110282

12. Jiang, H., Hu, X., Wang, T. and Sun, Z. (2021). Experimental and Numerical Study on Thin-Walled Hollow Bridge Piers. 820(1), pp.012004–012004. doi: https://doi.org/10.1088/1755-1315/820/1/012004.

13. Cao, X., Xu, Y., Kong, Z., Shen, H. and Zhong, W. (2017). Residual Stress of 800mpa High Strength Steel Welded T Section: Experimental Study. *Journal of Constructional Steel Research*, 131, pp.30–37. doi: https://doi.org/10.1016/j.jcsr.2016.12.001.

14. Rossini, N.S., Dassisti, M., Benyounis, K.Y. and Olabi, A.G. (2012). Methods of Measuring Residual Stresses in Components. *Materials & Design*, 35, pp.572–588. doi: https://doi.org/10.1016/j.matdes.2011.08.022.

15. Zhang, Z., Shi, G., Hou, L. and Zhou, L., 2021. Geometric Dimension and Imperfection Measurements of Box-T Section Columns Using 3D Scanning. *Journal of Constructional Steel Research*, *183*, p.106742. https://doi.org/10.1016/j.jcsr.2021.106742

16. Lyssakow, P., Friedrich, L., Krause, M., Dafnis, A. and Schröder, K.U., 2020. Contactless Geometric and Thickness Imperfection Measurement System for Thin-Walled Structures. *Measurement*, *150*, p.107038. https://doi.org/10.1016/j.measurement.2019.107038

17. Shi, G., Zhou, W., Bai, Y. and Lin, C. (2014). Local Buckling of 460mpa High Strength Steel Welded Section Stub Columns under Axial Compression. *Journal of Constructional Steel Research*, 100, pp.60–70. doi: https://doi.org/10.1016/j.jcsr.2014.04.027.

18. Kovacevic, S., Markovic, N., Sumarac, D. and Salatic, R., 2021. Unfavorable Geometric Imperfections in Steel Plate Girders Subjected to Localized Loads. *Thin-Walled Structures*, *161*, p.107412. https://doi.org/10.1016/j.tws.2020.107412

19. Sato, A., Mitsui, K., Aoyama, M., & Inden, A. K. (2017). Effect of Initial Imperfection on Elasto-Plastic Behavior of Square Steel Tubular Columns under Compressive Axial Force with Monotonic Antisymmetric Bending Moment. *Journal of Structural and Construction Engineering*, *82*(741), 1787-1797. https://doi.org/10.3130/aijs.82.1787

20. British Standards Institution (2022). *BS EN 1993-1-5. Eurocode 3. Design of Steel Structures*.

21. Susantha, K.A.S., Aoki, T. and Jayasinghe, M.T.R. (2007). Finite Element Analysis of Steel Columns Subjected to Bi-directional Cyclic Loads. *Engineer: Journal of the Institution of Engineers, Sri Lanka*, 40(4), p.35. doi:https://doi.org/10.4038/engineer.v40i4.7152.

22. Shen, C., P. Mamaghani, I.H., Mizuno, E. and Usami, T., 1995. Cyclic Behavior of Structural Steels. II: Theory. *Journal of Engineering Mechanics*, *121*(11), pp.1165-1172. https://doi.org/10.1061/(ASCE)0733-9399(1995)121:11(1165)

23. Yamao, T., Iwatsubo, K., Yamamuro, T., Ogushi, M. and Matsumura, S., 2002. Steel Bridge Piers with Inner Cruciform Plates under Cyclic Loading. *Thin-Walled Structures*, *40*(2), pp.183-197. https://doi.org/10.1016/S0263-8231(01)00059-3

24. Usami, T. and Kumar, S., 1996. Damage Evaluation in Steel Box Columns by Pseudodynamic Tests. *Journal of structural engineering*, *122*(6), pp.635-642. https://doi.org/10.1061/(ASCE)0733-9445(1996)122:6(635)

25. Usami, T. and Ge, H.B., 1998. Cyclic Behavior of Thin-Walled Steel Structures—Numerical Analysis. *Thin-walled structures*, *32*(1-3), pp.41-80. https://doi.org/10.1016/S0263-8231(98)00027-5

26. Zheng, Y., Usami, T. and Ge, H., 2000. Ductility Evaluation Procedure for Thin-Walled Steel Structures. *Journal of Structural Engineering*, *126*(11), pp.1312-1319. https://doi.org/10.1061/(ASCE)0733-9445(2000)126:11(1312)